THE ASTROPHYSICAL JOURNAL, 365:586–601, 1990 December 20

A SEARCH FOR SCALE-DEPENDENT MORPHOLOGY IN FIVE MOLECULAR CLOUD COMPLEXES

ROBERT L. DICKMAN,[1,2,3] MARK A. HORVATH,[1,3] AND MICHAEL MARGULIS[1,2,3]

Received 1990 February 23; accepted 1990 June 20

ABSTRACT

We have analyzed *IRAS* 100 μm intensity images and 60 μm optical depth maps of five molecular clouds complexes (Chameleon, R CrA, ρ Oph, Taurus, and the Lynds 134/183/1778 group) using the area-perimeter analysis previously applied to terrestrial clouds by Lovejoy, and Rys and Waldvogel, and to the *IRAS* infrared cirrus by Bazell and Désert. In agreement with these workers, we find that cloud areas are generally a noninteger power of perimeter. The projected two-dimensional shapes of these objects are thus fractal. A noise analysis indicates that this result is not an artifact but reflects a fundamental property of the clouds. As in the case of terrestrial clouds, the fractal geometry almost certainly arises from the action of turbulence.

Because turbulent fluctuations of equal energy might be expected to produce the most regular isodensity structure on the smallest scales within molecular clouds, we examine the dependence of fractal dimension on spatial scale in all five clouds. Even at the highest resolution of our analysis—approximately 0.3 pc—we find no evidence of completely smooth morphology. This implies that the correlation length of the turbulence driving the morphological irregularities within the clouds is less than 0.3 pc. However, we also find evidence of *trends* toward smoother geometries on smaller scales within the cloud complexes. This indicates either a decline in the amplitude of turbulent stress with scale (consistent with a correlation length not too far from the resolution of our analysis), the increasing dominance of self-gravity on smaller scales (as expected), or both.

We examine the compatibility of our results with the theory of Hentschel and Procaccia, which was formulated to deal with the fractal geometries of terrestrial clouds and which is based on modifications of the Kolmogorov model of fully developed, incompressible turbulence. We find inconsistencies between the theory and what is currently known about turbulence in molecular clouds.

Subject headings: interstellar: molecules — nebulae: structure — turbulence

I. INTRODUCTION

The physical processes which determine the structure of molecular clouds are complex. External pressure forces act upon the outer layers of the clouds in a spatially and temporally irregular manner, and the nonlinearity of the hydrodynamic equations which govern the internal structure of the clouds offers a rich potential for complex physical behavior. This complexity is reflected in the irregular morphology of interstellar clouds.

The competing roles of gravity and turbulence in determining cloud morphology are of particular interest in this connection. Within molecular clouds, denser, more tightly bound regions are usually associated with smaller spatial scales, implying that perturbations of equal energies will produce the most regular isodensity structures on the smallest scales. The presence of coherence scales in a turbulent cloud can be expected to have a similar effect: since the velocity and density fluctuations associated with turbulence approach zero on scales significantly smaller than the correlation length of the flow, the pressure field in regions of this size will be significantly smoother than on larger scales. This leads one to expect that cloud morphology will become blunter and more compact on the scale(s) at which turbulent fluctuations begin to smooth out. However, while such scales must generally exist in molecular clouds, present ignorance about the detailed kinematic state of molecular clouds makes the extent of their universality unclear. It is also unknown whether their attainment is generally gradual or abrupt: is the erasure of convoluted cloud structure on small scales a gradual process, or do fluctuating pressure forces suddenly "turn off" on some critical scale?

The lack of self-consistent theoretical models for molecular cloud dynamics suggests strongly that these issues be approached from an observational perspective. A general method which may be useful in studying cloud morphology has been developed by Mandelbrot (1977, 1983). In this approach, the degrees of "crinkliness" of cloud boundaries is quantified through the relationship between projected cloud area and perimeter. By studying the relationship between these two quantities at various density levels within a single cloud, one can probe the behavior of turbulence as a function of gravitational potential and spatial scale. In addition, by studying the relationship between area and perimeter for clouds of different sizes, one may be able to investigate from a phenomenological point of view the extent to which the physical processes which determine cloud shapes act universally.

In practice, the degree of perimeter contortion in a cloud is characterized by the quantity known as the Hausdorff dimension, D_H (Mandelbrot 1983), which appears in the relation Perimeter α Area$^{D_H/2}$. In general, D_H need not be an integer. As is well-known, Mandelbrot has designated objects with noninteger Hausdorff dimensions as *fractals*.

Lovejoy (1982) was the first to apply these concepts in a study of the projected two-dimensional shapes of terrestrial clouds and rain-producing cloud cells. He found that these

[1] Department of Physics and Astronomy, University of Massachusetts.
[2] Five College Radio Astronomy Observatory.
[3] Five College Astronomy Department.

objects can be characterized as fractals with $D_H \sim 1.35$, on size scales spanning three orders of magnitude, and noted that this result was very close to the value of 4/3 expected to characterize the dependence of the variance of pressure fluctuations with spatial separation in an atmosphere obeying Kolmogorov's theory of incompressible, homogeneous, isotropic turbulence. The fractal dimension of the projected cloud shapes thus appeared to reflect quite naturally the underlying physical mechanism responsible for shaping these objects, and its invariance over three orders of magnitude in length suggested strongly that both the outer (i.e., *energy-injection*) and inner (i.e., *dissipation*) scales of the Kolmogorov energy cascade lay outside the dimensions probed by the study.

Similar work was later carried out by Rys and Waldvogel (1986) using radar data on hail-producing clouds. On length scales between 10 and 100 km, they found a fractal cloud dimension essentially identical to that determined by Lovejoy and attributed the sharp break in fractal dimension below 10 km to the smoothing action of strong winds.

Bazell and Désert (1988, hereafter BD) applied these concepts to astronomical clouds, calculating the space-filling properties of 100 μm *IRAS* images of interstellar "cirrus" by using plots of the logarithm of projected cloud area versus logarithm of cloud perimeter. They determined $D_H = 1.26 \pm 0.03$ for three areas of the sky, a value consistent with the results of Lovejoy and Rys and Waldvogel. If universal, this result suggests intriguing and (somewhat surprising) parallels between the hydrodynamics of the Galactic intercloud medium, and the subsonic, and effectively incompressible, atmospheric flows which shape terrestrial clouds.

Because self-gravity is generally believed to be negligible in cirrus clouds (Blitz, Mundy, and Magnani 1984), these objects lack the potentially revealing and interesting complications which the addition of a gravitational field would provide. In this paper, we extend the work of BD to more massive and dense molecular clouds in order to investigate what changes (if any) a significant gravitational field produces in cloud morphology. By analyzing the relation between projected cloud area and perimeter at various equivalent dust column density levels in five rather different cloud complexes—Chameleon, Ophiuchus, Taurus, R Coronae Australis, and Lynds 134/183/1778—we also seek to establish whether a cloud's environment plays a role in determining its shape.

Our area-perimeter analysis is based on *IRAS* Sky Flux images. Owing to their large-scale coverage and uniform format, these are ideal resources for exploring cloud structure. Moreover, given the proximity of the clouds (all are believed to lie between 140 and 160 pc of the Sun[4]), the 2′ resolution of the Sky Flux data allows us to see down to a linear scale of ~ 0.09 pc. Our initial intention was to utilize 60 μm optical depth values determined from the 60 μm and 100 μm plates to trace each cloud, since it has been shown that τ_{60} correlates well with visual extinction up to $A_V \sim 10$ mag, except in the vicinity of embedded IR point sources (Jarrett, Dickman, and Herbst 1989). However, construction of an optical depth map requires the use of both 60 and 100 μm plates, and the presence of heavy striping and misregistrations associated with the joining of more than one plate, as well as the difficulty of removing large-scale zodiacal backgrounds for clouds located near the ecliptic plane, can lead to substantial inaccuracies in the resulting large-scale maps. Consequently, we also analyzed 100 μm intensity images alone, assuming the infrared emission to trace the column density of dust (Boulanger and Perault 1988; Cernicharo and Guélin 1987).

The outline of the remainder of this paper is as follows. In § II we explain our data reduction and background determination techniques. In § III, we give the results of our area-perimeter correlation studies for the 100 μm intensity and 60 μm optical depth images of each cloud; we also present an alternative method for calculating the Hausdorff dimensions of the clouds, and compare our results with those implied by the area-perimeter approach. Results are discussed in § IV, and the entire paper is summarized in § V. The paper also includes an Appendix, in which we explore the effects of image noise on determinations of Hausdorff dimension.

II. DATA AND DATA REDUCTION

a) *The Clouds*

Figures 1*a*–1*e* are gray scale renderings of the 100 μm maps of each region. Each cloud complex is described individually below. A catalog of the total mass of each cloud complex, as well as tabulations of the masses, positions, and sizes of the subclouds out of which the complexes are formed, are presented elsewhere (Horvath, Dickman, and Margulis 1990).

Chameleon: A visual inspection of *IRAS* Sky Flux plate 206 reveals that the complex has a morphology superficially similar to that of the infrared cirrus clouds. The cloud boundary is characterized by diffuse, wispy emission, giving the complex a windblown appearance. Chameleon is located out of both the Galactic plane ($l = 297°$, $b = 15°$) and the ecliptic (ecliptic latitude $-60°$), so that confusion by diffuse Galactic and zodiacal emission is minimized. Despite its irregular appearance, the Chameleon complex is a substantial, self-gravitating molecular cloud, approximately 20 pc across: Hyland, Jones, and Mitchell (1982) surveyed the most active star-forming region of the cloud in 2 μm, and found it to be a moderately active site of low-mass star birth. Our analysis is based on a section of the Sky Flux plate 1^h35^m wide in α and 4°12′ wide in δ, centered on $\alpha = 11^h07^m$, $\delta = -77°06'$.

Ophiuchus: The Ophiuchus complex is made up of several large cloud units (Loren 1989), forming a filamentary structure which stretches approximately 6° (32 pc) across the *IRAS* plates. The complex is currently an active site of low- to intermediate-mass star formation (Wilking and Lada 1983; Wilking *et al.* 1985), and has already produced a rich association of young stellar objects. The cloud is located off the Galactic plane ($l = 354°$, $b = 17°$) in the Upper Scorpius OB association, (de Geus 1989), but near the ecliptic plane (ecliptic latitude $\sim 4°$); zodiacal contamination was thus a concern in the background removal process required to determine the cloud optical depth at 60 μm (see Jarrett, Dickman, and Herbst 1989). The cloud area analyzed was the result of combining Sky Flux plates 159 and 161, and was 16° wide in α and 10° wide in δ, and centered on $\alpha = 16^h36^m$ and $\delta = -26°34'$.

Taurus: Because of the difficulties in establishing borders for the many clouds within this region, *IRAS* Sky Flux plate 51 was analyzed in its entirety. Ungerechts and Thaddeus (1987) have surveyed the cloud in CO and produced maps which include the entire region in our study. They find that the region contains many small cloud clumps, making it ideal for our analysis. The ecliptic and Galactic planes run directly through Taurus, so that background emission was a concern in generating the 60 μm opacity maps. As usual, the *IRAS* Sky Flux

[4] Recent work suggests a distance for the Chameleon clouds of some 200 pc, as opposed to the previous value of ~ 140 pc (K. Strom 1989, private communication).

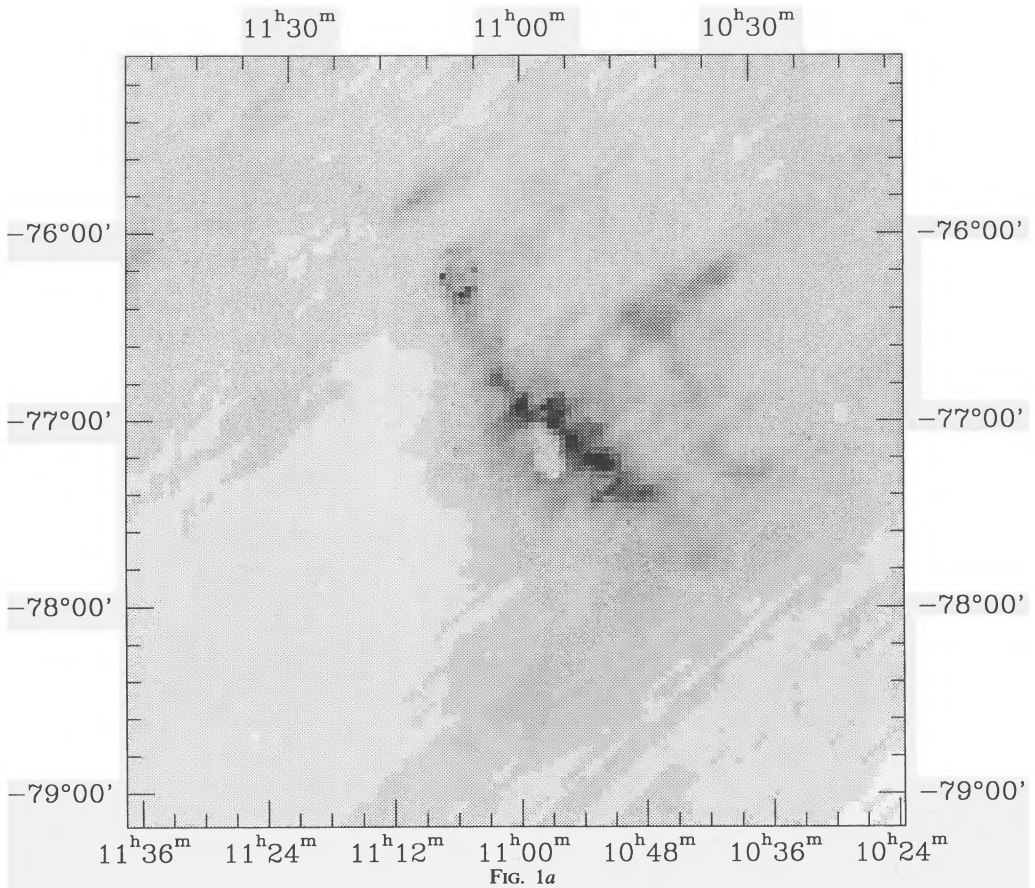

FIG. 1*a*

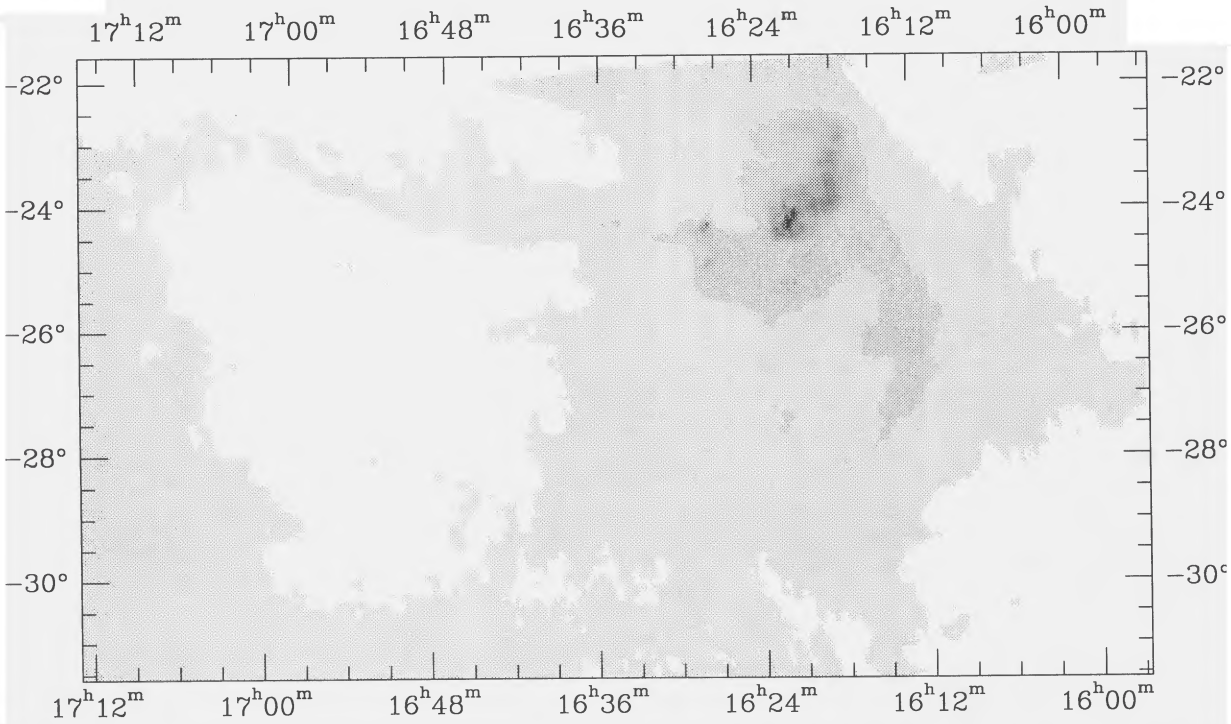

FIG. 1.—(*a*) Gray scale map of the Chameleon molecular cloud complex based on *IRAS* 100 μm Sky Flux data. (*b*) Gray scale map of *IRAS* 100 μm emission near the ρ Ophiuchi molecular cloud. (*c*) Gray scale map of *IRAS* 100 μm emission from much of the Taurus molecular cloud complex. (*d*) Gray scale map of the R Coronae Australis cloud. (*e*) Gray scale map of *IRAS* 100 μm emission in the vicinity of the dark clouds L134, L183 and L1778. Notice the heavy striping which appears in the map. This can also be seen in its effect on our results, because it tends to round and elongate large structures in the image, spuriously lowering Hausdorff dimension.

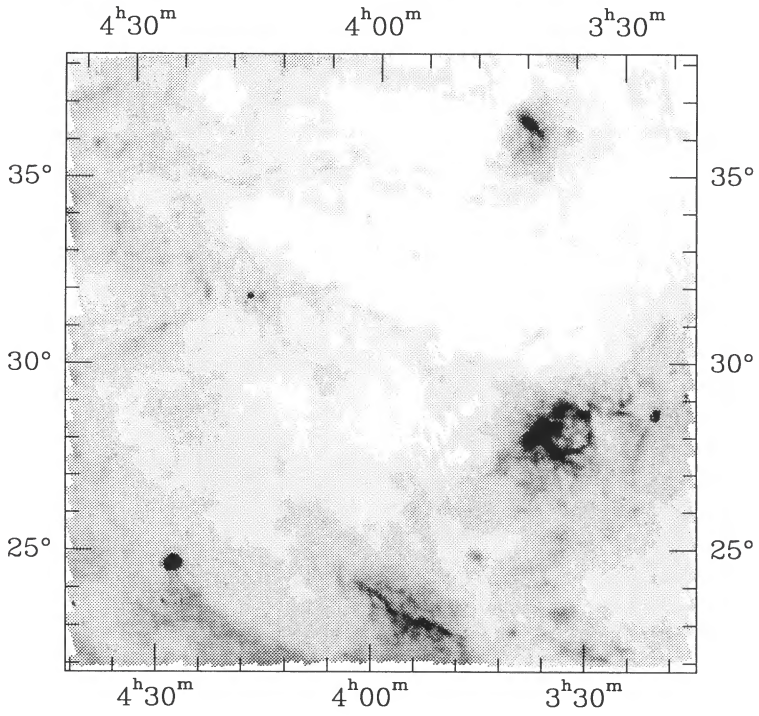

FIG. 1c

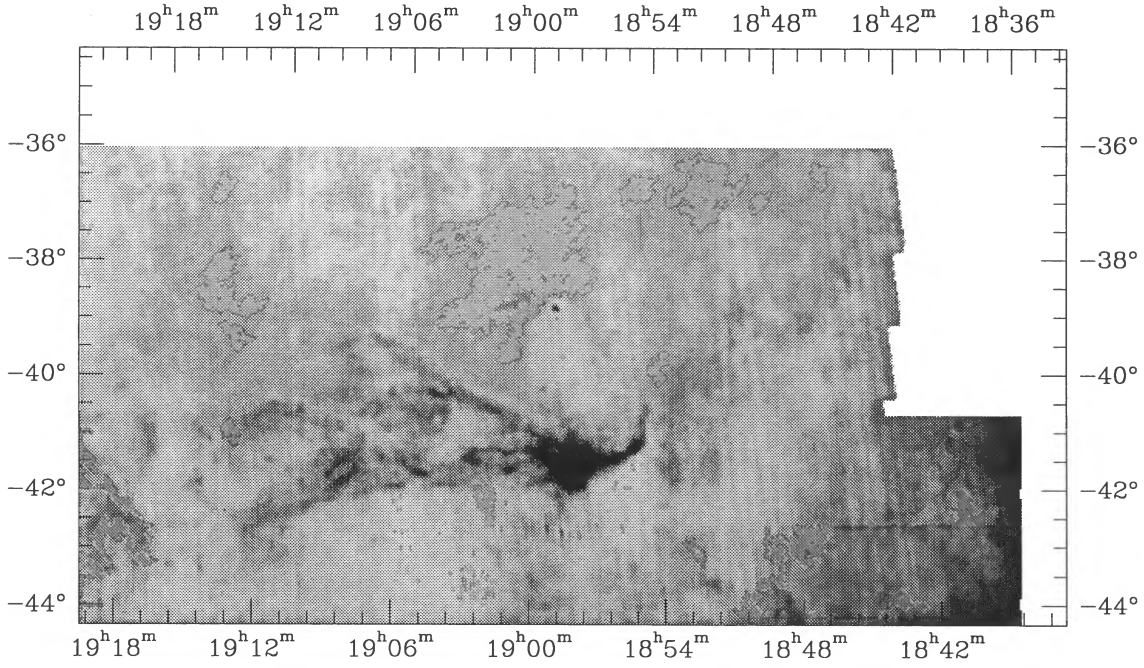

FIG. 1d

plate was 16°.5 wide on each side; it was centered at $\alpha = 4^h00^m$, $\delta = 30°00'$.

R Coronae Australis: Located 17° south of the Galactic plane, and at the same Galactic longitude as the ρ Ophiuchi cloud ($l = 355°$), the R CrA molecular cloud is also a well-studied star-formation site (Taylor and Storey 1984). Like Ophiuchus, R CrA has a central star-forming core surrounded by an irregular envelope of gas and dust nearly 30 pc across. Wilking *et al.* (1985) have surveyed the complex and established that it is devoid of high-mass star formation. R CrA spreads across two *IRAS* Sky Flux plates (162 and 183) which were combined into one image. The field studied was 10° in α by 16°.5 in δ, centered at $\alpha = 18^h58^m$, $\delta = -39°20'$.

Lynds 134/183/1778: This grouping of dark clouds from the Lynds catalog lies at high Galactic latitude ($b \sim 35°$) and is often considered to be part of single complex (Clark and Johnson 1981); L 183 is frequently designated "L134N" in the molecular cloud literature. Studies by Gilmore (1978) and

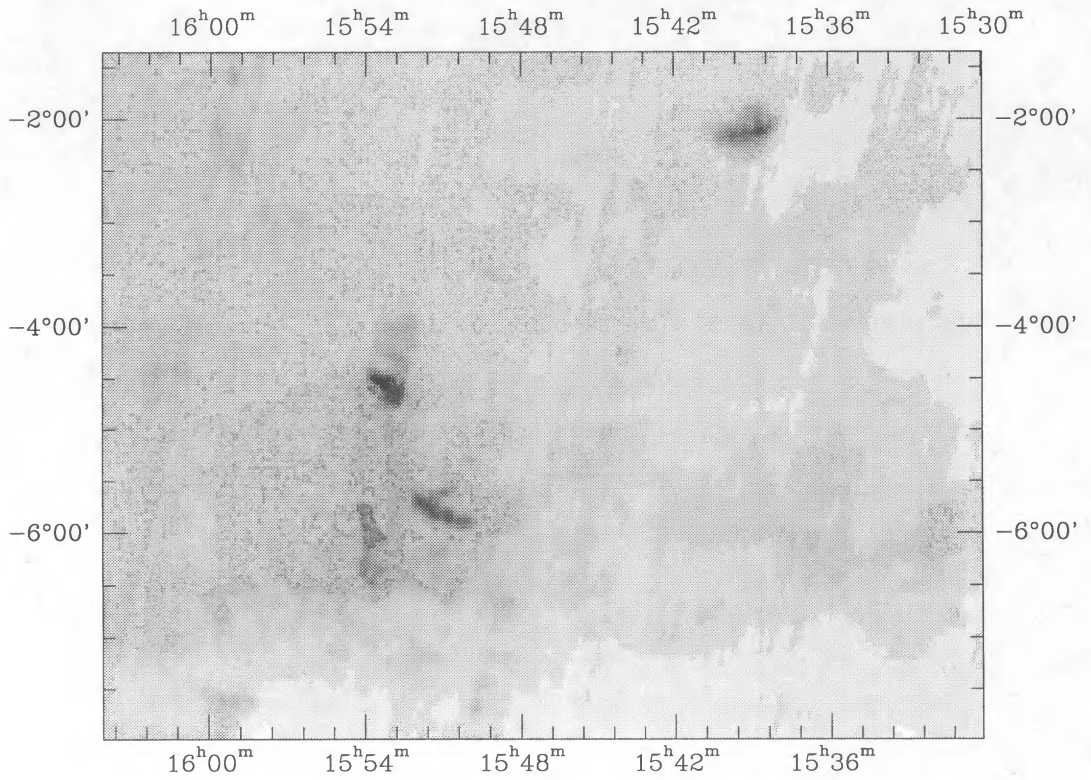

Sargent *et al.* (1983) reveal no evidence for embedded recently formed stars within these clouds. Likewise, there are no far-infrared sources listed in the *IRAS Point Source Catalog* which can be unambiguously associated with embedded young stellar objects; Swade (1987) concludes that L183 is either incapable of forming stars, or is in a stage of evolution which precedes the formation of protostars. Unfortunately, while the complex is an excellent candidate for our analysis, the 100 μm *IRAS* Sky Flux plate is heavily striped. Our efforts to destripe the plate while retaining the true morphology of the clouds are of uncertain quality, and our results for this complex are less secure than those for the other clouds. All data for the clouds come from a section of *IRAS* plate 111 centered at $\alpha = 15^h51^m$ and $\delta = -4°30'$, approximately 30^m wide in α and 8° long in δ.

b) *Background, Noise Determination, and Area-Perimeter Calculations*

The area-perimeter analysis of 100 μm images which we carry out in this work is completely insensitive to the presence of a *constant* background. However, the presence of a spatially variable background can bias the determination of the Hausdorff dimension, particularly on length scales characteristic of the background gradient, and therefore must be corrected for. Accordingly, with the exception of the Chameleon cloud (where the extreme weakness of the zodiacal background permits the subtraction of a constant background) a linear plane was fit to the 60 and 100 μm backgrounds in each data set. The planes were fit through points immediately adjacent to each cloud which were judged to be free of cloud material on the basis of a visual inspection of the Palomar prints. In order to avoid errors in the 60 μm optical depth determinations, identical locations were used to fit both 60 and 100 μm backgrounds.

The area-perimeter analysis described below requires specification of the rms random noise, σ, in each 100 μm image and optical depth map. Since there are large-scale gradients in both these quantities, this is not an entirely straightforward process. In the case of the 100 μm emission, σ was determined from the mean pixel-to-pixel variation of the weak emission in a region immediately adjacent to the cloud. In the case of the 60 μm optical depth maps, a rough estimate of the characteristic noise associated with pixel-to-pixel fluctuations in 60 and 100 μm brightness adjacent to the clouds was used to estimate the optical depth uncertainty at small values of τ_{60}. The nonlinear dependence of τ_{60} on intensity at $\lambda = 60$ and 100 μm implies that larger uncertainties will occur at higher optical depths, an issue which we discuss in § IV*a*.

Our analysis begins by identifying all simply connected[5] objects in each cloud field which have a 100 μm brightness or 60 μm opacity in excess of a given value. The area and perimeter of each object is then calculated, and the threshold for object identification is increased by three times the random rms noise level appropriate to each cloud field. The process is then repeated. All areas and perimeters in what follows are expressed in units of Sky Flux pixels, which are 2′ on a side; since the cloud complexes considered in this study all lie at about the same distance from the Sun, there is in all cases an approximately constant correspondence between linear scale and cloud perimeter. Following BD, only cloud units larger in

[5] Multiply connected structures were also identified by our search technique, but were excluded from subsequent analysis owing to their ill-defined perimeters: one could choose to define the perimeter solely as the length of the exterior boundary or as the sum of that quantity and the perimeter of all internal "holes." Disregarding all multiply connected objects has virtually no effect on our analysis, since simply connected clouds and clumps comprise well over 95% of all the objects detected in the five fields studied in this work.

TABLE 1

DETERMINATIONS OF $D_H/2$

Cloud	100 μm Data	τ_{60}	Coarse Resolution
Chameleon	0.639 ± 0.008	0.640 ± 0.006	0.602 ± 0.015
ρ Ophiuchi	0.587 ± 0.002	0.604 ± 0.001	0.610 ± 0.015
Taurus	0.615 ± 0.002	0.614 ± 0.004	0.620 ± 0.008
R CrA	0.623 ± 0.010	0.650 ± 0.003	0.591 ± 0.020
L 134/183/1778[a]	0.609 ± 0.020	0.616 ± 0.007	0.520 ± 0.011
⟨Bazell-Désert (1988)⟩	⟨0.63 ± 0.02⟩		

[a] Striping in data makes tabulated values uncertain.

area than 13 pixels are considered in the analysis, in order to avoid the spuriously smooth morphologies which would unavoidably be associated with objects composed of small numbers of square pixels.

III. RESULTS

Plots of log (Perimeter) versus log (Area) based on the 100 μm data for each cloud complex are shown in Figures 2*a*–2*e*. The wave patterns sometimes discernible in the plots are due to noise effects and are discussed in the Appendix. Plots for the τ_{60} data, which look similar, are not shown. As expected, the areas and perimeters are well-correlated.

We have used a least-squares fit to determine the slopes and intercepts of the plots for each complex (see § IV, eq. [1]). These are listed in Tables 1 and 2, along with the results of BD for comparison; the tables also contain the results of fitting the plots based on the 60 μm cloud optical depth maps. All quoted errors represent the standard error of the fits.

While we shall defer the physical interpretation of the log P versus log A plots to § IV, it is important to note here that many of the data points shown in Figures 2*a*–2*e* are not completely independent. For example, suppose that at our starting intensity level a cloud complex is made up of three simply connected units. As the intensity threshold for defining the clouds is raised there are two possible fates for each of these units: (1) They may maintain their identity as structural units. In that case, the log P versus log A values associated with increasing intensity thresholds will move steadily along the log P-log A plot and provide a measure of boundary convolution with increasing H_2 column density (and thus increasing gravitational potential). (2) At a particular intensity threshold, a cloud unit may abruptly split into two or more daughter cores. In this case, the trajectory of the cloud in the log P-log A plane will be discontinuous, and the (log P, log A) values for the cores can be regarded as at least somewhat independent of those for the parent object.

Because of the ambiguity associated with interpreting the log P versus log A plots as a property of a well-defined population of member clouds within each complex, we have supplemented our analysis with a second scheme that takes into account more closely the usual definition of a fractal.

Fractals are self-similar; that is, they possess a morphology that is invariant under a change of scale. To test whether the clouds in our sample possess this property, we analyzed the perimeter-area behavior of our Sky Flux plates at progressively worse resolutions. Using a Gaussian spatial filter, we smoothed the 100 μm images of the Chameleon, R CrA, and Lynds clouds to a resolution of 6′ pixel^{-1}, and the images of the Ophiuchus and Taurus clouds to 8′ pixel^{-1}. We then reran the area-perimeter analysis using the emission found at a single, representative brightness contour. The results are given in the fourth column of Table 1. Although the smaller number of data points associated with the use of a single intensity contour produces a larger formal error, the fitted slopes are consistent with the previous results.

IV. DISCUSSION

a) Behavior of D_H

The results above indicate that noninteger values of D_H are required to describe the projected two-dimensional morphology of the five molecular cloud complexes—that is, these objects appear to be fractal in shape. The Hausdorff dimensions determined for the cloud group exceed unity, indicating that cloud perimeters grow more rapidly with area than would be the case if condensations within the complexes were geometrically simple objects. However, noise can be expected to crenelate the perimeter of any cloud image. Before attempting to interpret our results physically, it is therefore first essential to establish that they are not an artifact of noise in the 60 and 100 μm *IRAS* images. This issue is explored in the Appendix, where a study of the effects of noise suggests that, although D_H in the complexes may be underestimated by $\sim 10\%$, our results do in fact indicate the presence of a legitimately fractal cloud geometry in all five cloud regions.

As indicated in Table 1, all three methods used to calculate the mean Hausdorff dimensions of the cloud complexes yield

TABLE 2

DETERMINATION OF INTERCEPTS AND AREA-PERIMETER PROPORTIONALITY CONSTANTS, K[a]

Cloud	100 μm Data	$K_{100\,\mu m}$	τ_{60}	K_τ
Chameleon	0.517 ± 0.017	0.394	0.548 ± 0.013	0.373
ρ Ophiuchi	0.580 ± 0.006	0.321	0.595 ± 0.003	0.321
Taurus	0.534 ± 0.004	0.367	0.562 ± 0.004	0.349
R CrA	0.573 ± 0.010	0.346	0.525 ± 0.006	0.395
L 134/183/1778[b]	0.597 ± 0.020	0.324	0.556 ± 0.014	0.354
⟨Bazell-Désert (1988)⟩	⟨0.43 ± 0.03⟩	⟨0.456⟩		

[a] $K = 10^{-b/D_H}$. See § IV.

[b] Striping in data makes values somewhat uncertain.

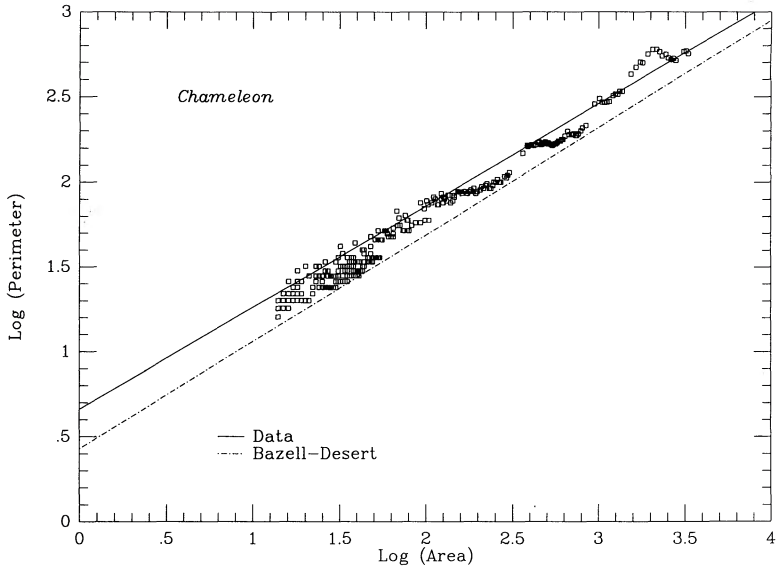

FIG. 2*a*

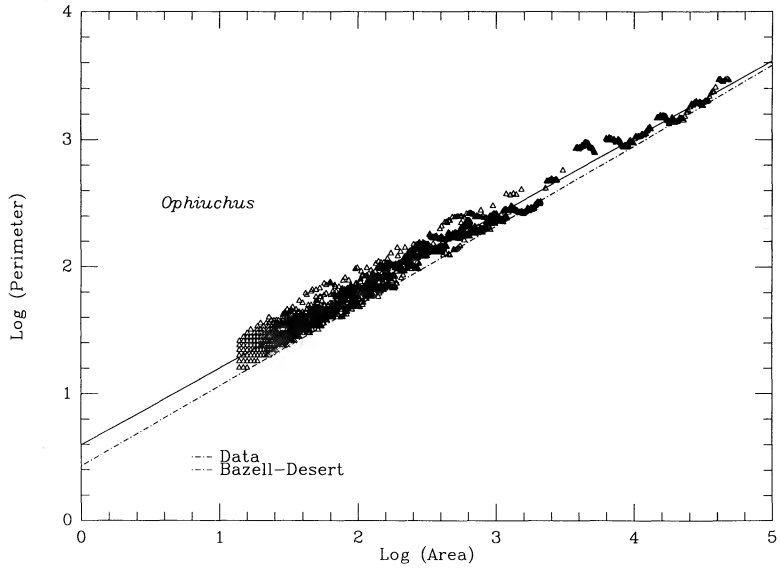

FIG. 2*b*

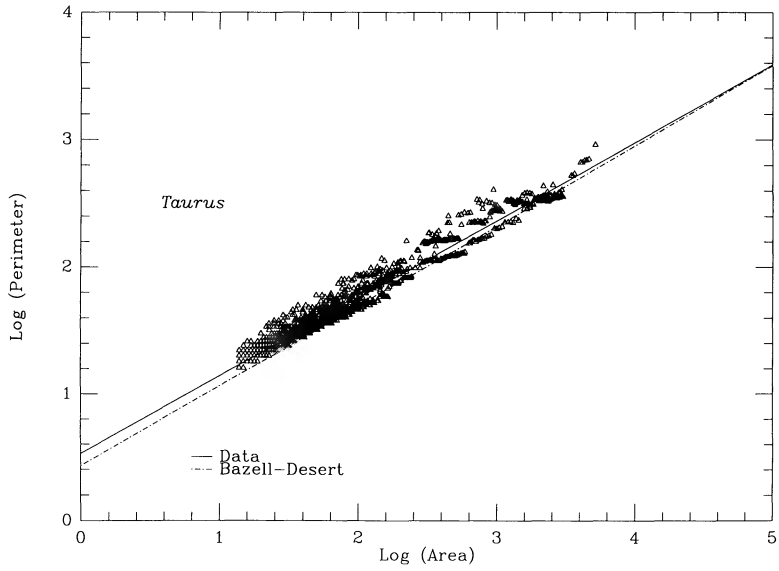

FIG. 2*c*

FIG. 2.—(*a*) log (Perimeter) vs. log (Area) plot for Chameleon based on 100 μm *IRAS* data. The best linear fit is denoted by a solid line, whereas the broken line shows the results of Bazell and Désert (1988). (*b*) Same as Fig. 2*a*, but for the ρ Oph cloud. (*c*) Same as Fig. 2*a*, but for the Taurus clouds. (*d*) Same as Fig. 2*a*, but for the R CrA clouds. (*e*) Same as Fig. 2*a*, but for the L134/183/1778 region.

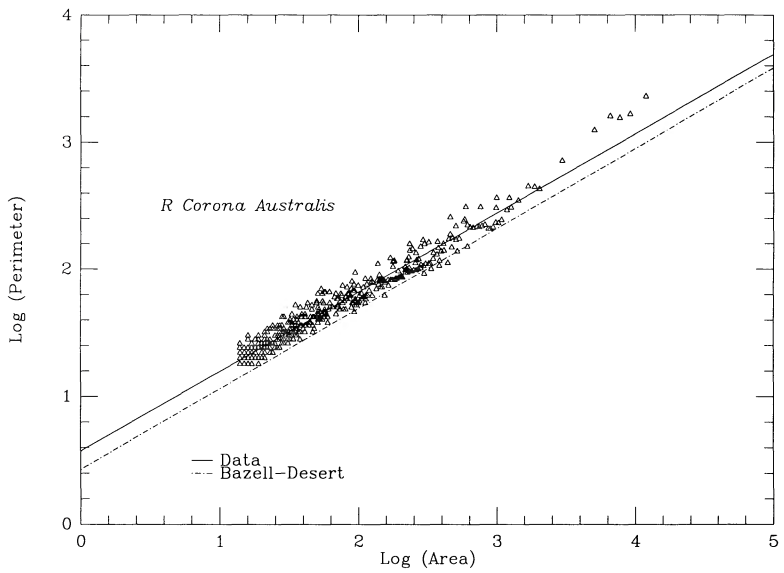

FIG. 2*d*

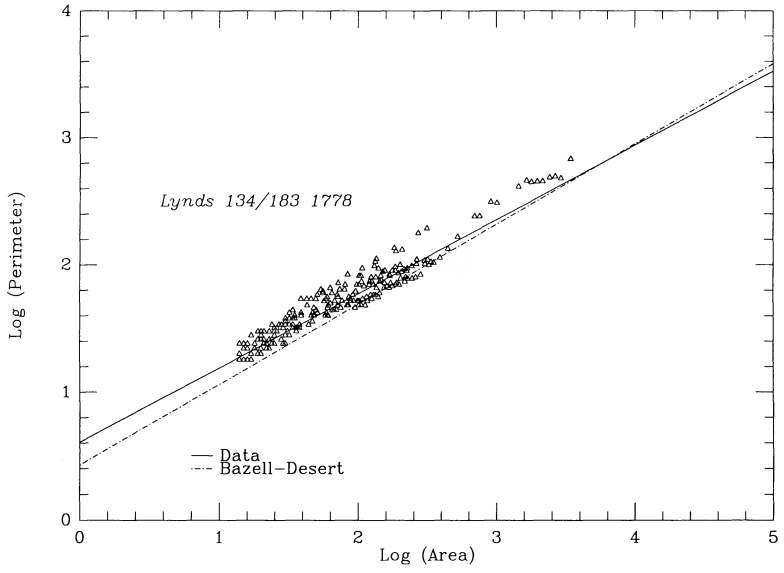

FIG. 2*e*

approximately the same value of D_H; with the exception of ρ Oph (discussed below), the dimensions determined for each complex from both the 100 m and τ_{60} maps lie within 3 σ of each other. Larger differences between both methods and various complexes are exhibited by the intercepts of the log A-log P plots (Table 2), and larger discrepancies are also associated in several instances with the mean D_H values calculated using the coarse resolution method. The fact that the latter method involves the preferential elimination of small structures in the ensemble suggests strongly that D_H may be scale-dependent in at least some of the cloud complexes.

To interpret these results, recall that the relationship between area, A, and perimeter, P, for a family of shapes can be written

$$A^{1/2} = KP^{1/D_H}, \tag{1}$$

where D_H is the Hausdorff dimension of the family and the constant K is characteristic of the shape. The intercepts, b, of the log P-log A plots already presented are thus related to D_H and K via

$$b = -D_H \log (K). \tag{2}$$

For example, all polygons and ellipses have $D_H = 1$, but quite distinct intercepts: squares have $b = \log 4$, whereas ellipses with major/minor axial ratios ϵ have

$$b = -\frac{1}{2} \log \left[\frac{\epsilon}{2\pi(1 + \epsilon)^2} \right]. \tag{3}$$

Although fractals will possess noninteger values of D_H, the constant K may still reflect their generalized shape: radially symmetric fractals will in general possess values of b larger than more elongated objects, in the same way that circles ($\epsilon = 1$) have b-values larger than ellipses ($\epsilon < 1$).

This simple expectation is clearly not borne out by the values of K listed in Table 2. While the Taurus, Ophiuchus,

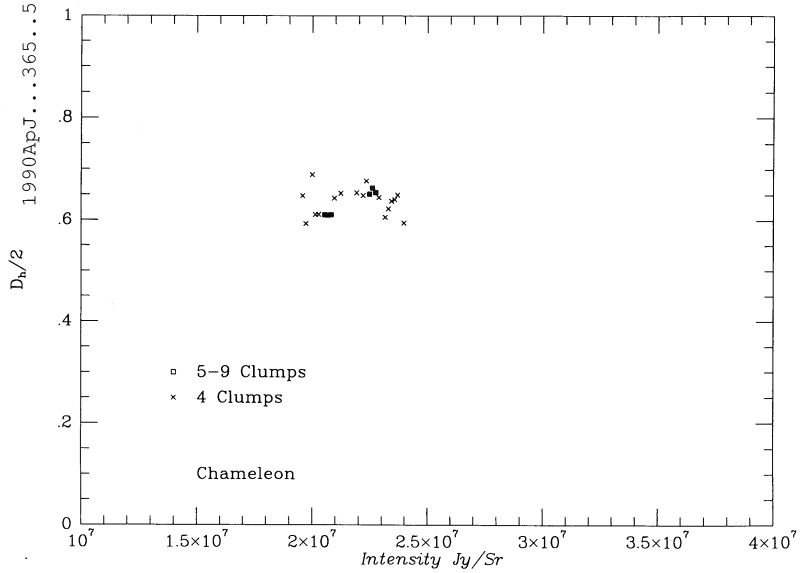

FIG. 3*a*

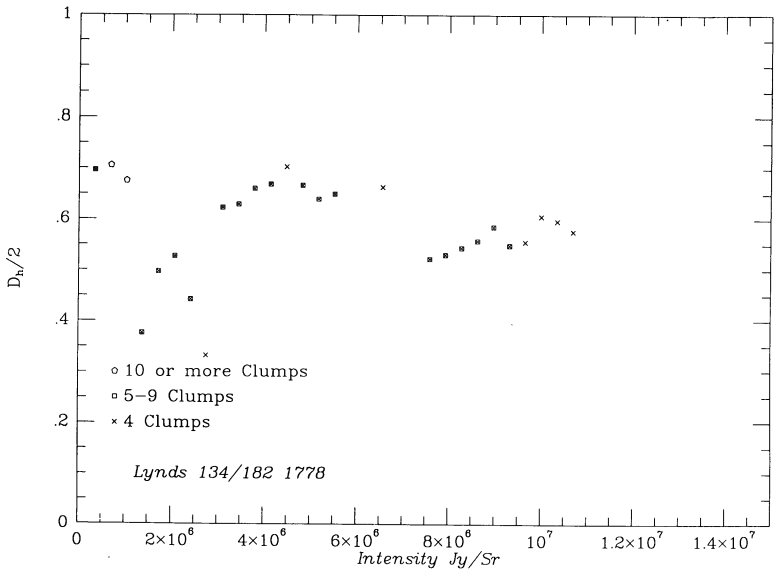

FIG. 3*b*

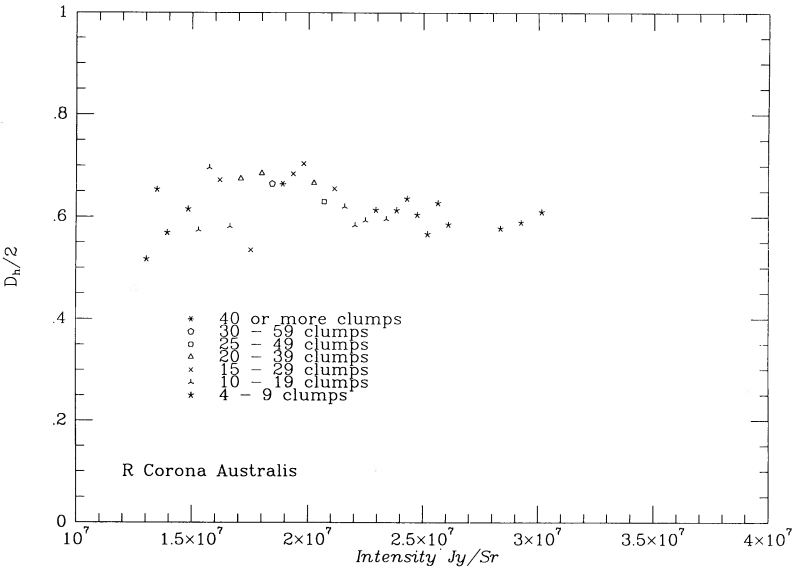

FIG. 3*c*

FIG. 3.—(*a*) Plot of best-fit $D_H/2$ at various 100 μm intensity thresholds for the Chameleon cloud complex (see § IV). (*b*) Same as Fig. 3*a*, but for the Lynds 134/183/1778 region. (*c*) Same as Fig. 3*a*, but for R CrA. (*d*) Same as Fig. 3*a*, but for the ρ Oph complex. (*e*) Same as Fig. 3*a*, but for the Taurus cloud complex.

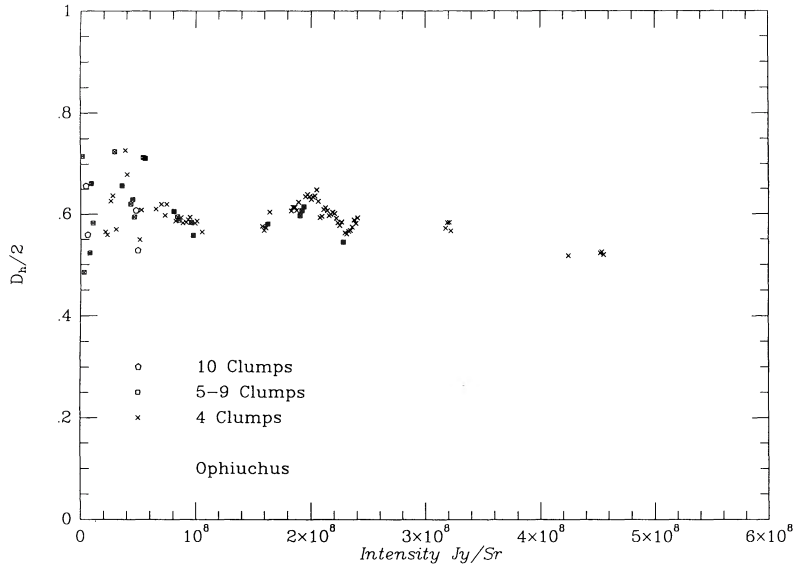

FIG. 3*d*

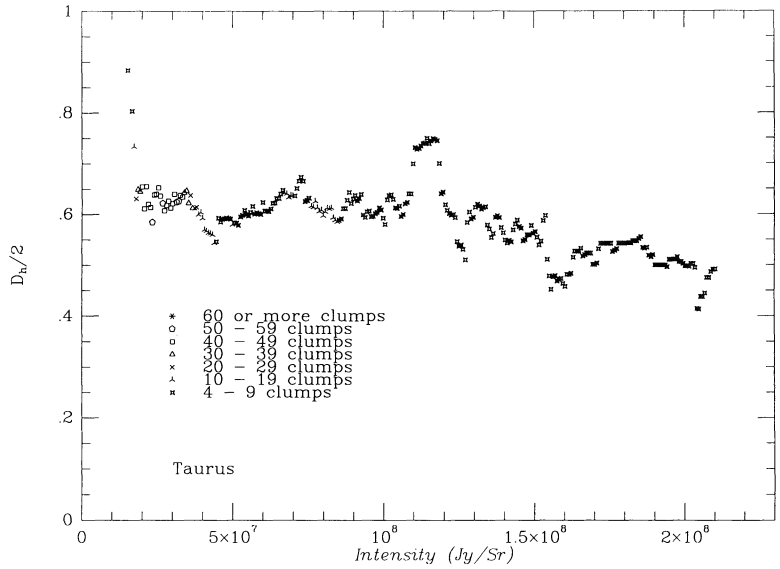

FIG. 3*e*

and R CrA complexes all possess strongly filamentary geometries on large scales, the values of K listed for these complexes in the Table are not, as a group, especially low (although K for ρ Oph *is* the lowest of all the tabulated values). This suggests that, despite the absence of clear evidence for a change in Hausdorff dimension with scale in Figures 2*a*–2*e*, the fractal properties of the clouds may nevertheless be scale-dependent to some degree. It is therefore desirable to scrutinize more closely the scale dependence of our results, as well as their relationship to local cloud density.

To do this, we evaluate the dependence of D_H upon extinction. That is, depending upon the particular data set under scrutiny, we evaluate the way in which the Hausdorff dimension depends upon either the 100 μm intensity or 60 μm opacity level at which it is calculated. We have already argued above that both measures can, within certain limits, be regarded as valid tracers of dust and gas column density. Inasmuch as elevated dust column densities in molecular clouds are usually associated with higher local densities and smaller spatial scales, this treatment is more or less equivalent to an explicit scale segregation.

Figures 3*a*–3*e* are graphs of $D_H/2$ versus 100 μm intensity level for each complex. Each value of D_H shown is the result of a least-squares fit of log P-log A data at each 100 μm brightness level containing four or more cloud components. Different symbols denote the number of cloud components on which each fit is based.

Because the *absolute* background in the 100 μm images is not well-determined (our only criterion being to produce a *flat* background), even an approximate quantitative relationship between $I_{100\,\mu m}$ and extinction or gas column density cannot be given for our images. This is not the case for Figures 4*a*–4*c*, where we have plotted $D_H/2$ versus τ_{60} for the R CrA, ρ Oph, and Taurus clouds. Here, the relationship found by Jarrett, Dickman, and Herbst (1989),

$$A_v = 6700\tau_{60} + 2.1\ , \qquad (4)$$

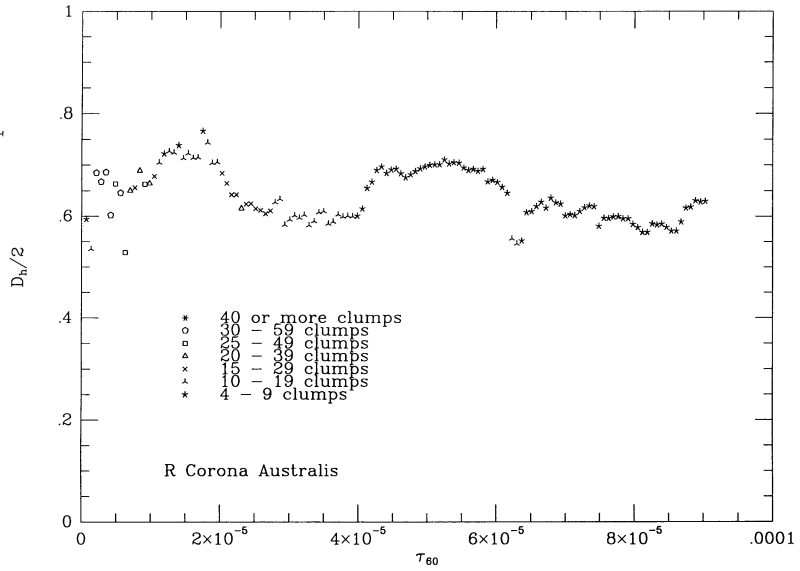

FIG. 4*a*

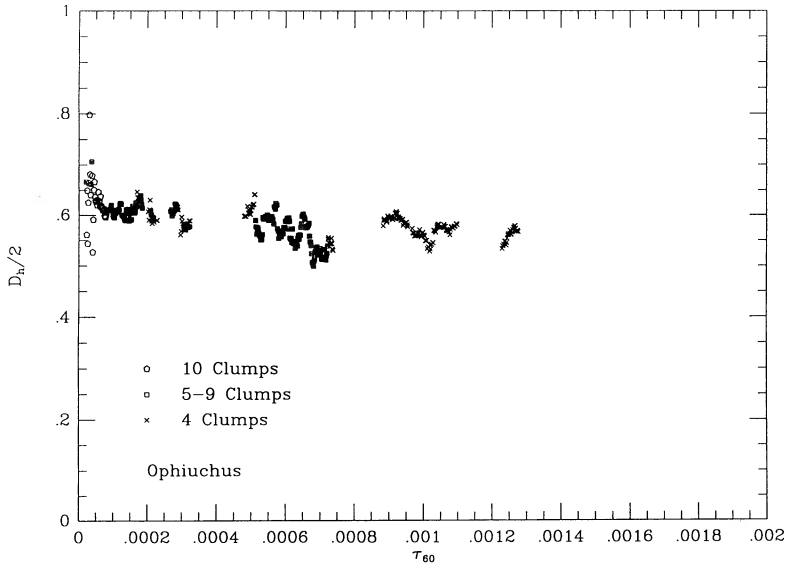

FIG. 4*b*

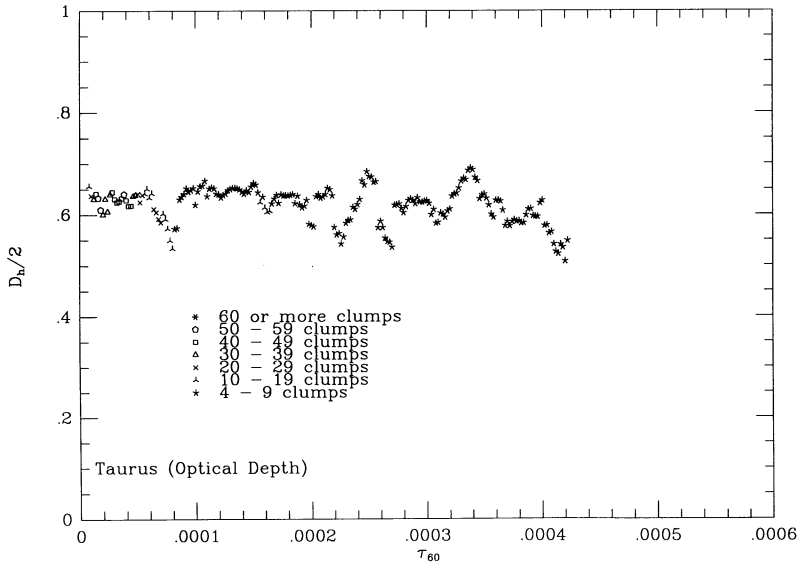

FIG. 4*c*

FIG. 4.—(*a*) Best-fit $D_H/2$ vs. τ_{60} for the R CrA clouds (see § IV). (*b*) Same as Fig. 4*a*, but for the ρ Oph clouds. (*c*) Same as Fig. 4*a*, but for the Taurus complex.

supplemented by the usual gas-to-extinction ratio (Bohlin, Savage, and Drake 1978; Dickman 1988), may be used as a guide (although its applicability to all five complexes here has, of course, not been established). The much greater number of data points in Figures 4*a*–4*c* as compared to Figures 3*a*–3*e* arises because our determination of the optical depth noise spacing was made in the outer parts of the clouds; our opacity spacings are highly conservative in the cloud interiors.

In the case of Chameleon, the 100 μm data set (Fig. 3*a*) yields a value of $D_H/2 \sim 0.65$ with relatively small scatter. The clustering of data points along the x-axis of the plot reflects the rather low dynamic range of the 100 μm Sky Flux image of the cloud, and the mean value is consistent with both the original analysis and the coarse resolution study. Although the optical depth image of the cloud complex has more dynamic range, the cloud is too unfragmented to yield more than about 3–4 subcondensations at each opacity threshold; as a consequence, least-squares fits to D_H at each selected value of τ_{60} are too noisy to be trustworthy, and we have therefore not plotted the behavior of $D_H/2$ versus 60 μm optical depth for this region.

The Lynds complex (Fig. 3*b*) is also limited in dynamic range and degree of fragmentation; as a result, only the variation of $D_H/2$ with $I_{100\,\mu m}$ intensity is plotted. The heavy striping of the image (§ II) renders the results in the plot somewhat untrustworthy, particularly at large scales: striping causes cloud boundaries to elongate along the stripes and tends to make ellipses out of inherently more irregular boundaries, especially those associated with large areas and perimeters. This effect can be discerned in Figure 2*e*, where a fit for $D_H/2$ on large scales yields a slope of just 0.51; this result is inconsistent with the value associated with the outer envelopes of the molecular clouds studied here, as well as with the results of BD for diffuse cirrus. However, in spite of this, it can be seen in Figures 1*e* and 2*e* that if the large outer areas of the cloud are ignored, the data look much more like Chameleon and R CrA than Ophiuchus or Taurus. This impression is confirmed by the fact that the average D_H derived from the 100 μm data for this complex (Table 1) does not differ significantly from those for the other cloud groups.

The dynamic range of the R CrA data is greater, and the cloud more fragmented than Chameleon. In both the $I_{100\,\mu m}$ and τ_{60} data sets (Figs. 3*c* and 4*a*), there is a suggestion of more compact morphology at higher equivalent visual extinction (and thus higher local gas densities), but the Hausdorff dimension associated with even the smallest condensations never approaches that of a simple, smooth shape ($D_H/2 = 0.5$).

Data for the ρ Ophiuchi complex have a dynamic range much larger than those of the Chameleon complex, and the range of values for $D_H/2$ is also larger (Figs. 3*d* and 4*b*). A general trend of decreasing $D_H/2$ with increasing $I_{100\,\mu m}$ and $\tau_{60\,\mu m}$ is suggested in both plots, with most of the data having a mean value ~ 0.60, although the trend is well-defined only in Figure 4*b*; most of the impression of a trend in Figure 3*d* is produced by the small cluster of data points in the 100 μm plot with a mean $D_H/2 = 0.51$, points which are isolated from the rest of the data by their high intensity (and therefore large A_V). This is the behavior one would expect for clumps whose geometry is smoothed by strong gravitational effects, but the effect is far less clear in the plot of Hausdorff dimensions versus τ_{60}.

In both plots, gaps in the data occur when the number of cloud clumps above the selection threshold is too small for a reliable determination of Hausdorff dimension; the data resume after large clumps fragment into enough daughters to make determination of D_H reliable again. Thus, the isolation of the points having $D_H/2 \sim 0.5$ in Figure 3*d*, as well as the sharpness of the change in Hausdorff dimension, suggests that the data points are associated with a steep and abrupt change in the 100 μm intensity of a number of distinct, localized regions, i.e., in several locally heated regions surrounding embedded point sources. Because the heating due to an embedded source is apt to be radially symmetric, the presence of a very smooth object in the 100 μm image of any molecular cloud must be regarded as a largely irrelevant structural feature due to local heating, unless its existence can be confirmed on an optical depth map. Even then, heating effects can compromise the validity of the simple opacity computed from 60 and 100 μm *IRAS* data (Jarrett, Dickman, and Herbst 1989), and the morphology inferred from an optical depth map may be compromised. In any case, the absence in Figure 4*b* of isolated data points with $D_H/2$ close to 0.5 indicates that, although the ρ Oph data show evidence for increasingly smooth morphology on smaller scales and higher densities, the structure of the cloud remains quite irregular and fractal on even the smallest scales resolved by our data.

Data for the Taurus complex are plotted in Figures 3*e* and 4*c*. While the 100 μm data suggest a smooth, fairly continuous decline in $D_H/2$ to an average ~ 0.5, the optical depth plot, which accounts more correctly for the influence of localized heating, shows no values of Hausdorff dimension this small; in fact, the change in D_H with opacity is barely significant. We therefore conclude that, as in Ophiuchus, there is no evidence for the presence of highly smoothed small-scale morphology in the Taurus complex on the scales probed by our data.

b) Implications

There is no significant evidence in our data that completely smooth morphologies—i.e., clumps and condensations characterized by $D_H/2 = 0.5$—are attained within any of the molecular cloud complexes studied here on linear scales as small as those corresponding to $\sqrt{13} \times 2' \sim 0.3$ pc. However, in two of the five complexes, ρ Oph and R CrA, there is strong evidence of a *trend* of increasingly smoother morphology on progressively smaller scales, and there is weak evidence for such a trend in the Taurus complex as well. Only in the Lynds cloud complex, where the data are corrupted by heavy striping, and in Chameleon, where there was relatively little dynamic range in the *IRAS* data, was no trend visible. Given the limitations of the data, our results clearly cannot exclude the presence of a trend in these regions.

There seems little doubt that the noninteger Hausdorff dimensions which characterize the clouds studied here reflect the presence of well-developed turbulent motions within these objects (Hentschel and Procaccia 1984). Since the local density fluctuations which produce the highly convoluted cloud structure associated with a fractal projected geometry must vanish on scales smaller than the correlation length of the density field, we may therefore conclude that *the correlation length of density fluctuations in a typical molecular cloud is less than about 0.3 pc.* This conclusion applies to relatively quiescent objects like the Lynds clouds and the Taurus and Chameleon complexes, as well as to more active star-formation sites such as the ρ Oph and R CrA clouds. While it is far from clear that the velocity and density coherence scales in a turbulent, self-gravitating cloud must be comparable in size, it is perhaps worth noting that Kleiner and Dickman (1987) obtained a

velocity correlation length ~ 0.1 pc in the Taurus cloud complex, a value consistent with the result obtained in the present work.

It is more difficult to interpret the observed trend toward progressively smoother morphologies on smaller scales. Part of the difficulty is the lack of a clear and appropriate theoretical framework for describing the morphology of a turbulent, self-gravitating interstellar cloud. For terrestrial clouds, Hentschel and Procaccia (1984) have shown that the fractal dimension exhibited by a passive[6] scalar, such as a rain cloud embedded in a turbulent flow, can be related to the velocity structure function of the turbulence. In discussing the geometry of terrestrial rain clouds implied by the results of Lovejoy (1982), they suggest that intermittency effects will cause the structure function to depart from the Kolmogorov 2/3 law behavior expected to characterize subsonic, incompressible turbulence (see, for example, Batchelor 1953; for an astronomically-oriented review of concepts and terminology, see Dickman 1985); the Richardson 4/3 law, relating the mean ensemble interparticle separation, would also be modified. Hentschel and Procaccia go on to suggest a theory of turbulent diffusion for calculating the deviations from these idealized laws, which can also be used to determine the Hausdorff dimension of objects such as rain clouds. Although the theory is essentially *ad hoc*, and does not treat the additional complexity which would be entailed by the inclusion of compressibility and self-gravity (both absolutely necessary features of any astronomical theory), it is of interest to test its applicability to the clouds studied in this work.

Hentschel and Procaccia find that the Hausdorff dimension of cloud shapes projected in two dimensions is

$$D_H = \frac{4}{3} + \frac{\mu}{6}, \tag{5}$$

where the constant μ is constrained by Lovejoy's observations of D_H to lie in the range $0.25 < \mu < 0.50$ for turbulence in the Earth's atmosphere. The theory also gives for the small-scale behavior of the velocity structure function, $S(l)$,

$$S(l) \sim l^{4/3 - \mu/3}. \tag{6}$$

Thus, in Hentschel and Procaccia's theory the structure function is predicted to vary with scale *less* steeply than in the Kolmogorov case. This is in sharp disagreement with the behavior of the velocity structure function found by Kleiner and Dickman (1987) for the Taurus molecular cloud complex, where on the smallest scales studied (~ 0.1–0.5 pc), the structure function varied *more* steeply than the Kolmogorov model would predict.

The lack of concordance between observation and the theory of Hentschel and Procaccia is perhaps unsurprising in view of the theory's neglect of compressibility and gravitational effects. Nonetheless, the lack of a reasonable theoretical context for interpreting the observational results is particularly troublesome, owing to the nonuniqueness of the Hausdorff dimension: very different physical processes can lead to virtually identical D_H, and it is generally untrue that the numerical closeness of two values of D_H implies near-identity of physics. This makes it nearly impossible to judge the implications of the fact that numerically similar Hausdorff dimensions characterize terrestrial clouds, interstellar cirrus, and dense molecular clouds, aside from noting that turbulent processes evidently play an important role in shaping all of these objects.

[6] A passive scalar is a quantity which participates in the turbulent flow without affecting it.

Finally, it should be kept in mind that astronomical data are themselves subject to inherent spatial and *ex post facto* filtering which can further complicate an interpretation of cloud geometry. Both infrared and radio maps of molecular clouds are constructed from data which necessarily average over structure smaller than the resolution scale, and the contouring routines which are sometimes used to identify clumpy structures are themselves spatial filters. These facts can render the Hausdorff dimension of a cloud image rather remote from the physical reality of the cloud itself. As an example, consider a model interstellar cloud made up of numerous clumps, each subtending a solid angle much smaller than that of the detector; such models have been invoked to describe giant molecular clouds on line-formation (Kwan and Sanders 1986) and astrochemical grounds (Taylor and Dickman 1989). It is a simple matter to construct such a model, in which individual clump locations are random, but where the number density of clumps rises toward the cloud center (Fig. 5). The model cloud can then be filtered to simulate its detection and mapping by a radio or infrared telescope (Fig. 6) provided the clumps are optically thin or do not shadow each other in phase space. Strikingly, an area-perimenter analysis of the model shown indicates that it possesses a Hausdorff dimension $D_H/2 \sim 0.65$. The exact dimension of the model cloud depends upon the number of clumps, essentially because its fractal structure arises from the random placement of the clumps, and can, of course, be made to approach unity by making the number of clumps extremely large (so that random $\sqrt{N}$ fluctuations become negligible).

We do not propose that actual molecular clouds resemble this highly schematic model. Its structure is far too *ad hoc* and remote from any plausible underlying dynamics to serve as a realistic paradigm of a dense interstellar cloud. However,

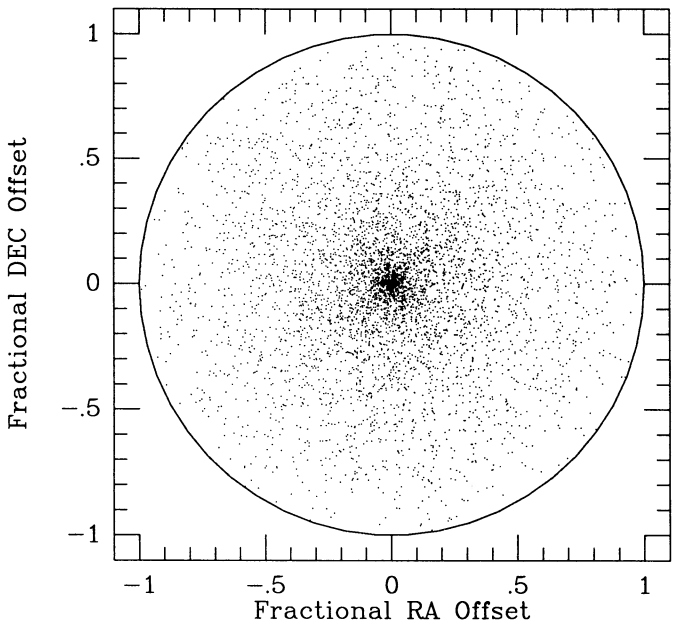

FIG. 5.—A centrally condensed model cloud which is made up of numerous, clumps. Models of this kind for giant molecular clouds have been suggested by Kwan and Sanders (1986) to resolve line formation problems, particularly with the millimeter lines of CO. The locations of the individual clumps are randomly chosen, but the number density of clumps increases toward the cloud center. For clarity, only 5000 points are plotted in the illustration, although 60,000 were modeled.

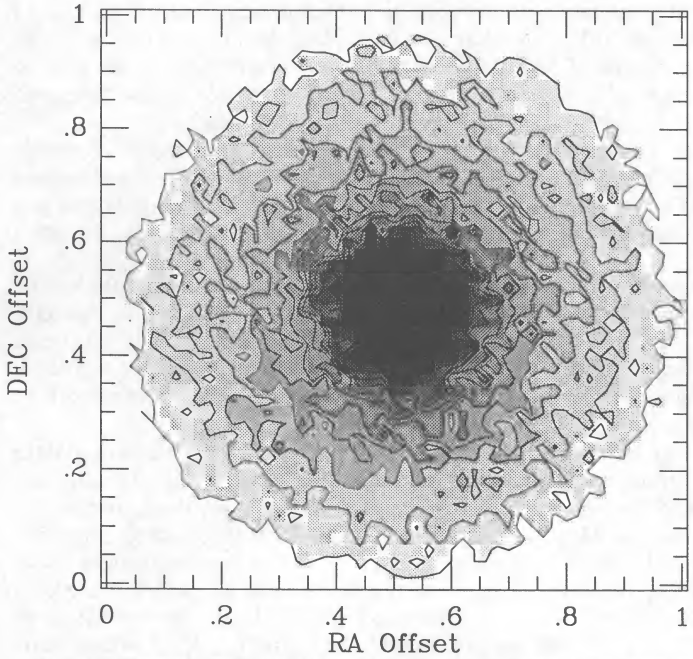

FIG. 6.—The spatially filtered image of the cloud which results if the model cloud is "mapped" in a raster pattern by an instrument with limited spatial resolution. A 51 × 51 square array was used to construct the image. Contours of the filtered intensity are also indicated. An area-perimeter analysis of the model image (§ III) yields a mean Hausdorff dimension for this model cloud of $D_H/2 \sim 0.65$.

extremely clumpy cloud structure *is* expected to develop from the density fluctuations associated with strong turbulence, and it is sobering that the essential simplicity of this model is obscured by the unavoidable filtering associated with the observing process.

These facts appear to make it unlikely that studies of the fractal structure of molecular clouds will be of use in clarifying the details of the physics responsible for the structure of these objects. Nevertheless, by studying the way in which the Hausdorff dimension of condensations within cloud complexes varies with scale size, one has the potential to clarify the scale-dependence of the turbulence which ultimately determines the physical structure of these objects. The structure of the clouds on small scales is of particular interest, since these lie closest to the star-formation process. Although the *IRAS* data on small scales are limited in resolution and subject to ambiguities related to embedded sources, geometrical techniques such as those used here may continue to be of value if applied to high-resolution molecular line maps.

V. SUMMARY AND CONCLUSIONS

The major results of this study are:

1. We have analyzed *IRAS* 100 μm intensity images and 60 μm optical depth maps of five molecular cloud complexes (Chameleon, R CrA, ρ Oph, Taurus, and the Lynds 134/183/1778 group) using the area-perimeter analysis previously applied to terrestrial clouds by Lovejoy (1982) and Rys and Waldvogel (1986), and to the *IRAS* infrared cirrus by Bazell and Désert (1988). In agreement with these workers, we have found that a noninteger Hausdorff dimension describes the shape of clouds and condensations within the complexes; that is, cloud areas are generally a noninteger power of perimeter, so that the projected two-dimensional shapes of these objects are "fractal" (Mandelbrot 1983).

2. We have analyzed the effect of noise on the cloud images and demonstrated that this result is not an artifact but reflects a fundamental irregularity of the clouds. As in the case of terrestrial clouds, it is likely that this arises from the action of turbulence.

3. The Hausdorff dimensions we find do not differ substantially from those found for terrestrial and interstellar cirrus clouds. Although our study did not include any regions of high-mass star formation, we find no dependence of cloud morphology on environment.

4. Because turbulent fluctuations of equal energy might be expected to produce the most regular isodensity structure on the smallest scales within molecular clouds, we examined the dependence of fractal dimension on spatial scale in all five clouds. Even at the highest resolution of our analysis—approximately 0.3 pc—we found no evidence of smooth morphology. This implies that *the correlation length of the turbulence driving the morphological irregularities within the clouds is less than 0.3 pc*. However, we also found strong evidence in two complexes of a measurable decline in Hausdorff dimension with decreasing scale. This indicates either a decline in the amplitude of turbulent stress with scale (consistent with a correlation length not too far from the resolution of our analysis), the increasing dominance of self-gravity on smaller scales (as expected), or both. There is weak evidence of a similar decline in a third complex, and no compelling evidence which would exclude its presence in the other two.

5. We emphasize that in the absence of a firm theoretical framework a specific interpretation of the Hausdorff dimensions obtained in this work is not possible: closeness of fractal dimension in two sets of objects does not guarantee near-identity of the physical processes responsible for their structure. The theory of Hentschel and Procaccia (1984)—formulated to deal with the fractal geometries of terrestrial clouds and based on modifications of Kolmogorov turbulence—was shown to be inconsistent with what is currently known about turbulence in molecular clouds.

This is contribution number 727 of the Five College Astronomy Department. Part of this research was supported by an *IRAS* guest investigator grant to R. L. D. R. L. D.'s work was also supported in part by NSF grant AST 88-15406 to Five College Radio Astronomy Observatory. We thank Karen Strom for useful discussions.

APPENDIX

COMPLICATIONS OF NOISE

The slopes of the log P versus log A plots in Figures 2*a*–2*e* suggest that molecular clouds can be described as fractal objects on scale sizes open to observation. However, noise will always tend to crenelate and lengthen an otherwise smooth boundary. Hence, before interpreting the noninteger D_H implied by our results in physical terms, we must first consider how our results may have been affected by random noise in the *IRAS* data.

The molecular clouds which we study in this work can be thought of as complex surfaces in a three-dimensional (α, δ, $I_{100\,\mu m}$) space. (For simplicity, we confine our remarks here to the 100 μm images, although what we say applies equally well to the 60 μm opacity maps.) In order to ascertain whether some (or all) of the area-perimeter complexity of the clouds originates in noise effects, we studied the effects of noise on a number of idealized nonfractal model cloud surfaces, including a pyramid, hemisphere, and ellipsoid in (α, δ, $I_{100\,\mu m}$) space.

In the absence of noise, a series of slices through each figure at various intensity levels produces a family of simple, nested nonfractal shapes (squares, circles, or ellipsoids) whose size decreases smoothly as the intensity threshold rises. Thus, subjecting these test objects to the area-perimeter analysis described in § III produced a log A-log P slope consistent with a Hausdorff dimension of unity. We then added specific amounts of Gaussian noise, with dispersion σ expressed as a fraction of the total intensity of the model cloud, to the shapes and studied their effects.

Even with addition of noise at the 0.0001% level, changes in the slope of the log A-log P plot were discernible: the fitted slope $D_H/2$ changed from 0.50 to 0.51. Furthermore, the log A-log P plot immediately acquired a waviness very reminiscent of the data plotted in Figure 2 (see especially Figs. 2*a* and 2*b*). This is shown in Figure 7 for the series of nested square model clouds; although the data are still fitted reasonably well by a line, there are some significant deviations at the low-area end. As more noise was added, the size of the waves and the *mean* slope of the log A-log P fit line began to increase markedly, but in a highly nonsystematic fashion: points in the log A-log P plane began to segregate into two separated groups, each having a distinctly different slope.

Because of the square's unrealistically sharp edges, all further noise modeling was carried out on hemispherical or ellipsoidal data surfaces. The first hemisphere modeled had a dynamic range of 100 intensity units and a spatial radius of 45 pixels; the intensity gradient was therefore relatively steep. Adding small amounts of noise, less than 2% of the dynamic range or so, then produced a mean slope to the log A-log P plot that was *lower* than the noise-free value of $D_H/2 = 0.5$; indeed, all the hemispheres and ellipsoids modeled produced ensemble mean Hausdorff dimensions lower than the value of unity possessed by the underlying model cloud geometries. However, as in the case of the square, the average value of D_H is not lowered uniformly across all scales as the noise level increases. Instead, the data fall into distinct groups with recognizably different slopes, as shown in Figure 8. Least-squares fits show that the slope of the upper end of curves is nearly $D_H/2 = 0.5$, whereas the slope of the lower end (where smaller cloud components are most drastically affected by the addition of noise) is nearly $D_H = 1$. Data at the lower part of the plots in fact represents nearly pure noise, with few large-scale correlated structures. In the limiting case, where a model image were made up completely of noise, the log A-log P plot would show a slope of unity everywhere.

The same pattern of reduced average D_H in the presence of noise, with two distinct slope populations was also found in the case of the ellipsoidal models, which leads us to conclude that *the addition of even a small amount of noise will cause cloud data to resolve into two discrete groups.*

We also investigated the relation of noise level to intensity gradient in producing a given degree of population bifurcation and mean slope distortion. While no simple relation could be established, it was clear that the steeper the intensity gradient, the larger the effect of a given fractional noise level would be.

Although the range of geometries explored in these simple model studies is not particularly large, two major conclusions emerge from our studies of the effect of random noise on a log P/log A analysis. First, noise can produce systematic waves in the trajectory of a single object in the log P/log A plane as the intensity threshold is systematically varied. These waves have obvious counterparts in the data shown in Figure 2, which describe the molecular clouds studied in this paper. However, we have been unable to determine the precise mechanism responsible for these oscillations. Second, noise is highly unlikely to be the source of the noninteger values of D_H found for the molecular cloud complexes: the effect of noise contamination on any underlying circular or ellipsoidal cloud geometries which might naively be expected to be present in molecular cloud complexes would be to produce a pair of distinct populations in a log P/log A plot, and, in our simulations, always produced a mean ensemble Hausdorff dimension of less than unity. This result is in clear contrast to the values greater than 1 found without exception for the real clouds.

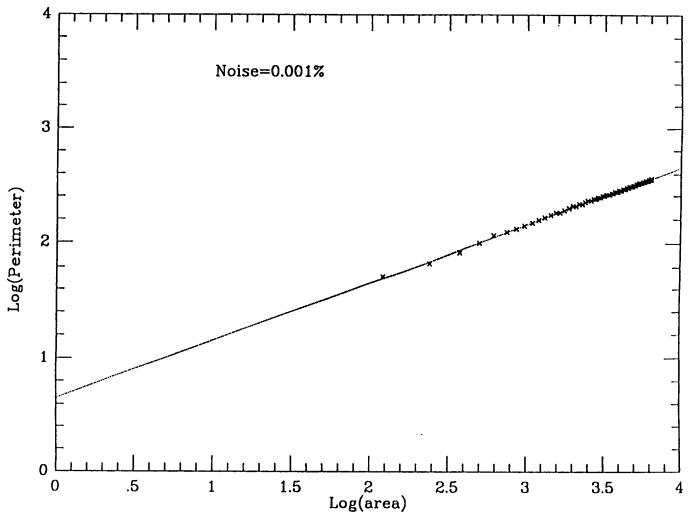

FIG. 7.—Log P vs. log A plot for a family of squares with noise 0.001% of peak intensity added (see Appendix)

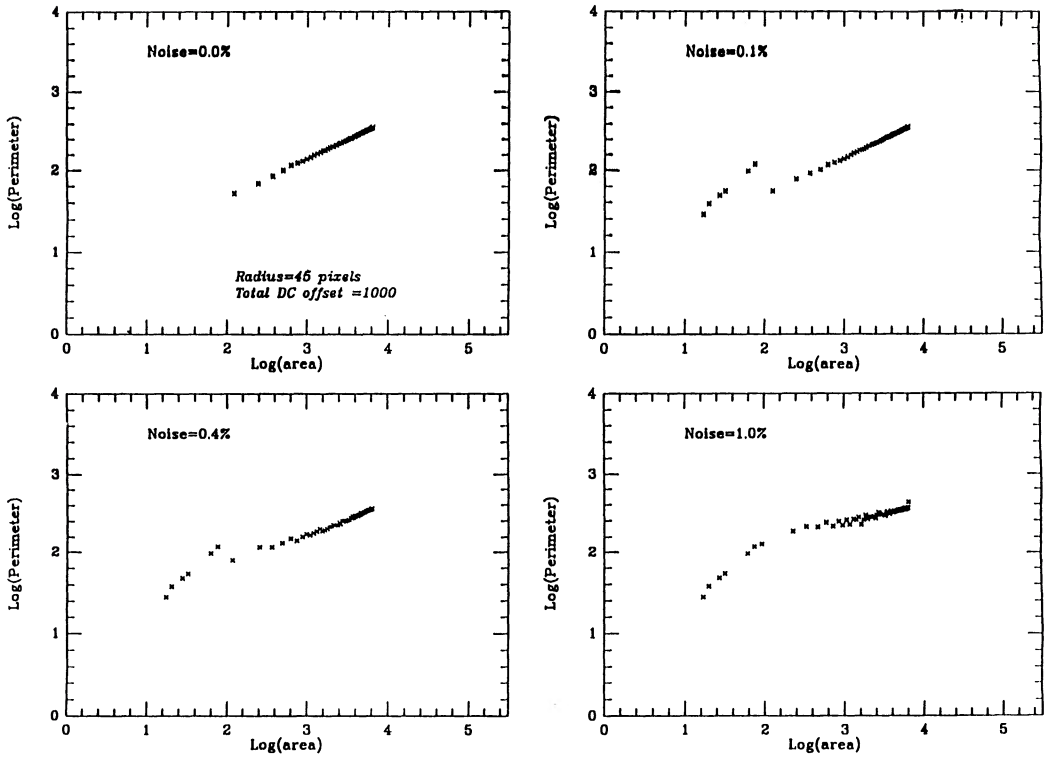

FIG. 8.—The progressive evolution of log P vs. log A as small amounts of noise are added to a model hemispheric data surface 45 pixels in radius. The points at the low-area end of each graph are due to noise, and are described by $D_H = 0.95$; those at the upper end possess the dimension of the original hemisphere.

REFERENCES

Batchelor, G. K. 1953, *The Theory of Homogeneous Turbulence* (Cambridge: Cambridge University Press).
Bazell, D., and Désert, F. X. 1988, *Ap. J.*, **333**, 353 (BD).
Blitz, L., Mundy, L., and Magnani, L. 1984, *Ap. J. (Letters)*, **282**, L9.
Bohlin, R. C., Savage, B. D., and Drake, J. F. 1978, *Ap. J.*, **224**, 132.
Boulanger, F., and Perault, M. 1988, *Ap. J.*, **330**, 964.
Cernicharo, J., and Guélin, M. 1987, *Astr. Ap.*, **176**, 299.
Clark, F. O., and Johnson, D. R. 1981, *Ap. J.*, **247**, 104.
deGeus, E. 1989, Ph.D. thesis, Leiden University.
Dickman, R. L. 1985, in *Protostars and Planets: II*, ed. D. C. Black and M. S. Matthews (Tucson: University of Arizona Press), p. 150.
———. 1988, in *Molecular Clouds in the Milky Way and External Galaxies*, ed. R. Dickman, R. Snell, and J. Young (Berlin: Springer), p. 55.
Gilmore, W. 1978, Ph.D. thesis, University of Maryland.
Hentschel, H., and Procaccia, I. 1984, *Phys. Rev. A*, **29**, 1461.
Horvath, M. A., Dickman, R. L., and Margulis, M. 1990, in preparation.
Hyland, A. R., Jones, T. J., and Mitchell, R. M. 1982, *M.N.R.A.S.*, **201**, 1095.
Jarrett, T. H., Dickman, R. L., and Herbst, W. 1989, *Ap. J.*, **345**, 881.
Kleiner, S. K., and Dickman, R. L. 1987, *Ap. J.*, **312**, 837.
Kwan, J., and Sanders, D. B. 1986, *Ap. J.*, **309**, 783.
Loren, R. B. 1989, *Ap. J.*, **338**, 925.
Lovejoy, S. 1982, *Science*, **216**, 185.
Mandelbrot, B. B. 1977, *Fractals* (San Francisco: W. H. Freeman).
———. 1983, *The Fractal Geometry of Nature* (San Francisco: W. H. Freeman).
Perault, M. 1988, in *Molecular Clouds in the Milky Way and External Galaxies*, ed. R. Dickman, R. Snell, and J. Young (Berlin: Springer), p. 233.
Rys, F. S., and Waldvogel, A. 1986, in *Fractals in Physics*, ed. L. Pietronero and G. Tosatti (Amsterdam: Elsevier Science Publications), p. 461.
Sargent, A. I., van Diunen, R. J., North, H. L., Fridlund, C. V. M., Alders, J. W. G., and Beinford, D. 1983, *A.J.*, **88**, 88.
Scalo, J. 1987, in *Interstellar Processes*, ed. D. J. Hollenbach and H. A. Thronson (Dordrecht: Reidel), p. 349.
Swade, D. 1987, Ph.D. thesis, University of Massachusetts.
Taylor, D. K., and Dickman, R. L. 1989, *Ap. J.*, **341**, 293.
Taylor, K. N. R., and Storey, J. W. V. 1984, *M.N.R.A.S.*, **209**, 50.
Ungerechts, H., and Thaddeus, P. 1987, *Ap. J. Suppl.*, **63**, 645.
Wilking, B. A., Harvey, P. M., Joy, M., Hyland, A. R., and Jones, T. J. 1985, *Ap. J.*, **293**, 165.
Wilking, B. A., and Lada, C. J. 1983, *Ap. J.*, **274**, 698.

ROBERT L. DICKMAN, MARK A. HORVATH, and MICHAEL MARGULIS: Radio Astronomy, LGRT 629-I, University of Massachusetts, Amherst, MA 01003